The magnetic activity cycle of II Pegasi: results from twenty-five years of wide-band photometry

M. Rodonò[1,2], S. Messina[1], A.F. Lanza[2], G. Cutispoto[2], and L. Teriaca[1]

[1] Dipartimento di Fisica e Astronomia, Università di Catania, Via S.Sofia, 78, 95125 Catania, Italy
[2] Osservatorio Astrofisico di Catania, Via S.Sofia, 78, 95125 Catania, Italy

Abstract. We present an analysis of a sequence of light curves of the RS CVn-type binary II Pegasi extending from 1974 to 1998. The distribution of the spotted area versus longitude is derived by Maximum Entropy and Tikhonov regularized maps, assuming a constant spot temperature (Lanza et al. 1998a). The spot pattern on the active K2 IV star can be subdivided into a component uniformly distributed in longitude and a second unevenly distributed component, which is responsible for the observed photometric modulation. The uniformly distributed component appears to be possibly modulated with an activity cycle of ~ 13.5 yr. The unevenly distributed component is mainly concentrated around three major active longitudes. The spot activity appears practically permanent at one longitude, but the spot area changes with a cycle of ~ 9.5 yr. On the contrary, the spot activity is discontinuous at the other two longitudes, and it switches back and forth between them with a cycle of ~ 6.8 yr. However, before each switching is completed, a transition phase of ~ 1.05 yr, during which both longitudes are active, occurs. After this transient phase, spot activity remains localized at one of the two longitudes for ~ 4.7 yr untill another switching event occurs, which re-establishes spot activity at the other longitude. The longitude separation between the permanent and the switching active longitudes is closest during the switching phases and it varies along the ~ 6.8 yr cycle. Different time scales characterize the activity at the permanent longitude and at the switching longitudes: a period of ~ 9.5 yr is related to the activity cycle at the permanent longitude, and a period of ~ 4.3 yr characterizes the spot life time at the switching longitudes in between switching events.

The photometric period of the active star changes from season to season with a relative amplitude of 1.5% and a period of ~ 4.7 yr. Such a variation of the photometric period may be likely associated with the phase shift of the light curves produced by the switching of spot activity from one active longitude to the other. The permanently active longitude shows a steady migration towards decreasing orbital phases, with an oscillating migration rate along the 9.5 yr cycle period and nearly in phase with the variation of its spotted area. The amplitude of the differential rotation derived from such a behaviour is of the order of $\sim 0.023\%$, about one order of magnitude smaller than esti-mated by Henry et al. (1995). The other two active longitudes migrates also towards decreasing orbital phase, but at a discontinuous rate. There appears to be no correlation between the location of the active longitudes with respect to the line joining the two components of the system and their activity level.

1. Introduction

II Pegasi (HD 224085) is a chromospherically active non eclipsing SB1 binary classified by Rucinski (1977) as K2–3 IV-V. Chugainov (1976) discovered II Peg to be variable at the optical wavelengths with a period of ~ 6.71 days. He interpreted the observed wave-like variability in terms of cool photospheric spots, orders of magnitudes larger than on the Sun, whose visibility was modulated by the stellar rotation. Subsequent multicolor photometric and spectroscopic studies by Vogt (1981) showed the characteristic variability of RS CVn systems. Indeed, II Peg is among the most active RS CVn binaries with light curve amplitudes up to 0.5 mag (cf. Strassmeier et al. 1997). Another interesting aspect of the magnetic activity manifestation on II Peg is the remarkable long-term change of the mean light level and the evidence collected from the Harvard plate archive on a solar-like Maunder minimum with almost null activity between 1900 and 1940 (Hartmann et al. 1979), when light curve amplitudes became apparent.

Estimates of the spotted area and temperature are available from several spectroscopic studies (i.e., Nations & Ramsey 1981, Poe & Eaton 1985, Rodonò et al. 1986, Byrne & Marang 1987), from the detection and modelling of TiO bands (Vogt 1981, Huenemoerder & Ramsey 1987, Neff et al. 1995) and from OH absorption excess (O'Neal & Neff 1997). The Hα and other chromospheric lines are in emission. Systematic monitoring of the Hα equivalent width shows clear evidence of rotational modulation, with the Hα flux anticorrelated with the photospheric flux, as expected in the case of spatial association between photospheric spots and chromospheric plages (Bopp & Noah 1980). The high activity level of II Peg has also been

Table 1. Mid epoch (HJD−2440000), time range, number of observing nights and sources of the light curves.

Mid epoch	HJD range	N_m	Source	Mid epoch	HJD range	N_m	Source
2044.08	2029.16-2078.17	9	Chugainov (1976)	7558.58	7556.08-7561.08	6	Mohin & Raveendran (1993)
2305.50	2278.35-2336.25	32	Chugainov (1976)	7731.83	7699.59-7748.55	19	Cutispoto et al. (1989);
3080.49	3076.12-3087.16	22	Rucinski (1977)				Doyle et al. (1992)
3379.74	3355.93-3444.75	11	Vogt (1981)	7784.92	7755.54-7811.39	11	Doyle et al. (1992)
4175.30	4168.24-4180.17	12	Nations & Ramsey (1981)	7853.54	7838.32-7878.17	16	Doyle et al. (1992);
4251.70	4236.10-4271.11	15	Raveendran et al. (1981)				Mohin & Raveendran (1993)
4472.25	4458.89-4485.60	12	Bohusz & Udalski (1981);				Phoenix-25
			Hall & Henry (1983)	8110.62	8095.54-8137.57	11	Doyle et al. (1993)
4501.62	4486.34-4513.73	30	Bohusz & Udalski (1981);	8185.67	8178.86-8191.82	12	Phoenix-25
			Hall & Henry (1983)	8229.47	8206.78-8272.60	16	Phoenix-25
4539.57	4514.26-4555.86	6	Bohusz & Udalski (1981);	8455.72	8427.97-8479.53	17	Byrne et al. (1995);
			Hall & Henry (1983)				Phoenix-25
4866.47	4846.86-4873.75	18	Lines et al. (1983);	8511.94	8480.56-8565.43	26	Byrne et al. (1995)
			Rodonò et al. (1986)	8551.97	8532.83-8573.75	24	Byrne et al. (1995);
4885.99	4875.43-4901.69	27	Lines et al. (1983);				Phoenix-25
			Henry (1983);	8646.01	8623.60-8652.57	7	Phoenix-25
			Rodonò et al. (1986)	8806.65	8802.94-8809.92	7	Phoenix-25
4932.19	4903.68-4977.60	15	Lines et al. (1983);	8896.75	8846.52-8928.80	21	APT-80; Phoenix-25
			Henry (1983);	8951.99	8948.39-8955.71	16	Phoenix-25
			Rodonò et al. (1986)	9171.82	9160.97-9195.92	8	Phoenix-25
5164.12	5120.93-5196.85	17	Henry (1983);	9264.51	9250.87-9279.49	32	APT-80; Phoenix-25
			Andrews et al. (1988)	9329.74	9299.74-9364.60	18	Phoenix-25
5340.95	5318.24-5358.29	16	Andrews et al. (1988)	9565.73	9541.54-9586.59	15	APT-80
5568.37	5535.58-5591.47	24	Evren (1988)	9629.12	9607.47-9660.52	18	APT-80
5607.86	5592.37-5624.39	19	Evren (1988)	9690.21	9676.36-9715.34	14	APT-80
5904.29	5896.63-5909.56	11	Evren (1988);	9898.57	9878.93-9911.60	20	APT-80; Phoenix-25
			Byrne & Marang (1987)	9994.23	9981.82-10008.43	35	APT-80; Phoenix-25
5935.83	5922.59-5948.56	22	Evren (1988);	10046.01	10014.72-10074.31	39	APT-80; Phoenix-25
			Byrne & Marang (1987);	10266.15	10247.56-10279.52	16	APT-80
			Kaluzny (1984)	10294.53	10289.55-10299.50	9	APT-80
5997.05	5971.80-6012.72	25	Strassmeier et al. (1989)	10308.80	10299.50-10315.48	11	APT-80
6043.55	6014.71-6098.59	19	Strassmeier et al. (1989)	10389.13	10392.70-10398.51	20	APT-80
6233.84	6223.96-6245.96	19	Strassmeier et al. (1989)	10417.83	10401.65-10430.27	30	APT-80; Phoenix-25
6281.82	6248.90-6307.82	26	Strassmeier et al. (1989)	10443.68	10436.23-10454.60	16	Phoenix-25
6327.17	6312.83-6339.78	18	Strassmeier et al. (1989)	10468.77	10457.59-10481.58	11	Phoenix-25
6358.84	6341.78-6372.75	23	Strassmeier et al. (1989)	10616.40	10596.96-10634.87	33	Phoenix-25
6382.18	6373.75-6391.73	12	Strassmeier et al. (1989)	10672.77	10644.46-10703.53	37	APT-80
6714.76	6678.62-6752.29	38	Cutispoto et al. (1987);	10727.56	10714.78-10724.49	28	APT-80
			Byrne & Marang (1987)	10766.41	10740.46-10805.33	38	APT-80; Phoenix-25
6819.87	6801.13-6832.10	24	Mohin & Raveendran (1993);	10827.14	10814.60-10842.59	11	Phoenix-25
			Strassmeier et al. (1989)	10983.88	10966.95-10996.91	22	Phoenix-25
7186.69	7175.09-7203.10	10	Mohin & Raveendran (1993)	11111.65	11093.38-11127.44	15	APT-80
7487.76	7441.86-7536.63	30	Cutispoto et al. (1989)				

confirmed by the detection of both radio and optical flares (van den Oord & de Bruyn 1994, Byrne et al. 1995).

Extensive photoelectric photometry of II Peg has been carried out since its optical variability was discovered (see, among others, Strassmeier et al. 1989, Rodonò & Cutispoto 1992, Mohin & Raveendran 1993, and references therein). A long-term photometric study was presented by Henry et al. (1995), who applied a simple two-spot model to derive informations on the spot areal change and surface migration. They found evidence of long-lasting spots, with life times ranging from months to more than 6 yr, and an activity cycle of ~ 4.4 yr along with a less pronounced cycle of ~ 11 yr. Photometric period variations from season to season were also detected and interpreted in terms of differential rotation (Henry et al. 1995).

Berdyugina et al. (1998a, 1999) have recently obtained Doppler images of the photosphere of II Peg which are in agreement with the two-spot models of Henry et al. (1995), though much more detailed. They show that spots are mainly located at high latitudes, even if truly polar spots were not found. Moreover, their results, and also those by Berdyugina & Tuominen (1998), show that the activity on II Peg is confined around two active longitudes, with one usually more active than the other.

Spot activity switches from one active longitude to the other in a quasi-periodic fashion, with a cycle of ~ 4.65 yr.

In this paper, we present a novel study of the long-term variability of II Peg by using a recently developed approach of light curve modelling (Lanza et al. 1998a). We analyse the longest photometric data base of II Peg that is presently available (1974–1998), including 6 years of new observations we have obtained with the Catania and Phoenix APTs (cf. Sect. 2.2). In the following sections we present the available data-base and the analysis procedures we have adopted. Our results support the conclusions by Henry et al. (1995) and Berdyugina et al. (1998a, 1999) on the existence of an activity cycle and persistent active longitudes. However, the more extended time base and the more sophisticated spot modelling approach we have adopted allow us to improve previous results, and to find evidence for multi-periodic activity and a peculiar, though systematic, behaviour of active longitudes.

2. Observations

2.1. Historical photometry

In order to study the variability of II Peg on the longest possible time base, all the light curves available in the literature were collected and consistently reanalysed (cf. Table 1 and open diamonds of Fig. 1). We have considered only V-band light curves because they represent a more complete and homogeneous data set. The much less numerous B and U light curves do not add any independent information on the spot surface distribution. Differential photometry of II Peg was obtained in the past using different comparison stars. When the same comparison star was used, different values of its standard V-band magnitude were sometimes used to transform differential values into standard magnitudes (see Table 2). In order to obtain a homogeneous data set, all the measurements from the literature were converted into differential magnitudes with respect to the same comparison star, HD 223461. It is important to notice that when II Peg had been observed by different authors at the same epochs (see Table 1), slightly different values of its standard V magnitudes were usually reported, although the differences never exceeded 0.015 mag. Our aim was to guarantee that all the light curves in our data set be comparable with each other. To achieve such a result, we adjusted the magnitude of the comparison HD 223461, to minimize the systematic differences among light curves observed at the same epoch. In such a way a value of $V = 8.52$ was found for the V magnitude of HD 223461 and it was adopted to calibrate all the light curves. Such a value of the comparison star V magnitude is equal to the value we independently determined from our new differential photometry (cf. Sect. 2.2) and to the mean magnitude reported in the SIMBAD database. Finally, having recalibrated all the measurements in a consistent way, the differential magnitudes were converted into the standard magnitude scale. For the magnitudes collected from the literature, one single average data point, when more than one observation per night was available, was derived. Finally, as suggested by Vogt (1981) and Poe & Eaton (1985), we added a 0.15 mag offset to Chugainov's light curves, to correct a prob-

Table 2. The comparison stars adopted by different authors to observe II Peg and their V-band magnitudes. ΔV indicates that only differential magnitudes are given.

| Comparison Star	V_{mag} (mag)	Source
BD+274648	9.419	Rucinski (1977)
BD+274648	9.403	Vogt (1981)
HD 224016	8.52	Nations & Ramsey (1981)
HD 223094	6.957	Raveendran et al. (1981)
BD+274648	9.39	Bohusz & Udalski (1981)
BD+274648	ΔV	Hall & Henry (1983)
HD 224084	8.23	Rodonò et al. (1986)
BD+274648	ΔV	Henry (1983)
BD+274648	ΔV	Lines et al. (1983)
HD 224084	8.23	Andrews et al. (1988)
HD 224083	ΔV	Evren (1988)
HD 224084	8.245	Byrne & Marang (1987)
HD 224084	8.24	Kaluzny (1984)
HD 224930	ΔV	Strassmeier et al. (1989)
BD+274648	9.403	Cutispoto et al. (1987)
HD 223094	6.957	Mohin & Raveendran (1993)
HD 224084	8.245	Cutispoto et al. (1989)
HD 224084	8.24	Doyle et al. (1992, 1993)
BD+274648	8.403	Doyle et al. (1992)
HD 224084	8.23	Byrne et al. (1995)
HD 224016	8.52	APT-80 + Phoenix-25

able zero-point error in Chugainov's photometry. As a result of the above procedure, we believe that the standard magnitude values of our time series photometry are consistent up to the 0.01 mag level.

2.2. New photometry

The new photometry analysed in the present study (filled circles in Fig. 1) was collected by means of two Automated Photometric Telescopes (APT): the Phoenix-25 since 1990, and the APT-80 since late 1992. The Phoenix-25 is a 25-cm telescope located at the Franklin & Marshall College at Washington Camp. (AZ, USA) that feeds a single-channel photon counting photometer, equipped with an uncooled 1P21 photomultiplier and standard *UBV* filters (Boyd et al. 1984, Baliunas et al. 1985). The APT-80 is an 80-cm telescope located at the *M. G. Fracastoro* station of Catania Astrophysical Observatory on Mt. Etna (Italy) that feeds a single channel charge-integration photometer, equipped with an uncooled Hamamatzu R1414 SbCs photomultiplier and standard *UBV* filters (Rodonò & Cutispoto 1992, Messina 1998).

II Peg was observed differentially with the Phoenix-25 using HD 224016 as comparison star, and HD 223461 as check star. A description of the observation and reduction procedures of the II Peg photometry obtained with the Phoenix-25 can be found in Rodonò & Cutispoto (1992). The typical errors of the differential UBV photometry were found to be of the order of 0.01, 0.005 and 0.005 magnitudes, respectively.

II Peg (v) was observed with the APT-80 differentially with respect to the comparison star HD 224016 (c) and to the check
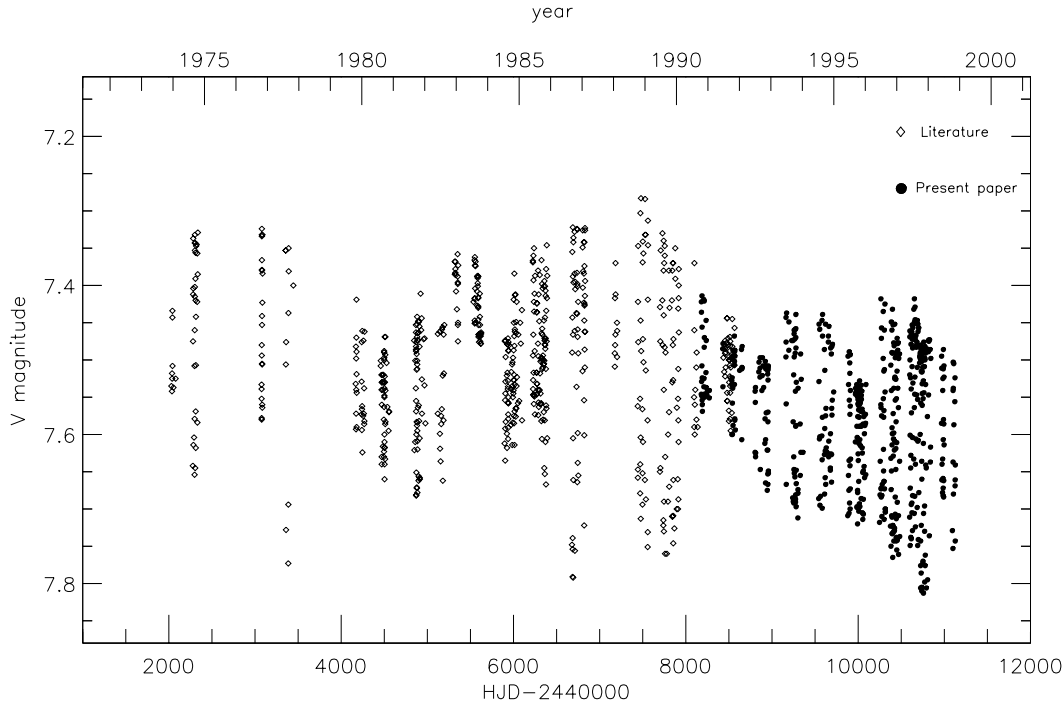
Fig. 1. V-band photometry of II Peg in the 1974–1998 interval. Open diamonds are the photometric data collected from the literature, filled circles are the newly presented photometry.

stars HD 223094 (ck1) and HD 224895 (ck2). The integration time in U, B and V filters was set to 15, 10 and 10 seconds, respectively, and the observing sequence was *n-c-ck1-c-v-v-v-c-v-v-v-c-ck2-c-n*, where the symbol n denotes the bright navigation star (HD 223461), which is the first star of the group the APT-80 hunts. The sky background was measured at a fixed position near each star. Differential magnitudes were corrected for atmospheric extinction and transformed into the standard UBV system. The transformation coefficients were determined quarterly by observing selected samples of standard stars. Due to the relatively short duration of an observing sequence ($\simeq 30$ minutes), the v−c, ck1−c, ck2−c and n-c values were finally averaged to obtain one single data point for each night. The transformation into the standard system is made with an accuracy of the order of 0.01, 0.01 and 0.02 mag in the V magnitude, B−V and U−B color indices, respectively. A comparison between the standard deviations of ck−c and v−c differential magnitudes shows that the comparison star has remained constant within the observation accuracy (Table 3).

3. Rotational modulation of the optical flux

Our complete data set ranges from 1974 to 1998 and consists of twenty seasons of data, that were individually analysed using the Scargle-Press period search routine (Scargle 1982, Horne & Baliunas 1986) to look for the period of the photometric modulation. The results of such an analysis are summarized in Table 4, where we present the covered time interval, the number of observations (N_m), the photometric period (P) and its uncertainty (ΔP), as derived by the method of Horne & Baliunas

(1986), the semiamplitude A of the fitting sinusoid of the optical modulation and the *false-alarm-probability* (FAP) of the peak frequency. This last quantity estimates the probability a peak of that height could result from a similar sample of Gaussian noise with the same variance of the analysed data (cf. Horne & Baliunas 1986). A search for secondary periodicities during each season was also performed by filtering the primary frequency modulation from the data and recomputing the periodogram for the residual data, according to the prescriptions of Horne & Baliunas (1986) and Baliunas et al. (1995). However, in none of the seasons we found significant evidence for a secondary periodicity in the optical modulation up to a FAP of 5% when the primary frequency is assumed to be real.

The photometric period showed changes from season to season in the range 6.688-6.770 days (see Fig. 7c) with an average value $\langle P \rangle = 6.726 \pm 0.022$ days. An analysis of such changes revealed that the photometric period may be cyclically variable, with a period of $\sim 4.7 \pm 0.15$ yr and a FAP=19%.

It was possible to select 67 time intervals during which the optical flux showed a regular modulation suggesting a quasi-stable spot pattern.

In such a way 67 light curves were obtained (Fig. 2), each labelled by the Julian date of the mid epoch of the corresponding observations (HJD−2400000, where HJD is the Heliocentric Julian Date). Since previous works (i.e., Berdyugina & Tuominen 1998) have shown that the active longitudes of II Peg do not possess a preferred orientation with respect to the line joining the centers of the binary components, the arbitrary initial epoch $HJD_0 = 2442025.5$ was adopted. In the present analysis, all the light curves have been phased using the ephemeris:

Table 3. Star, V magnitude, B−V and U−B colors, time range, number of observing nights and integrations per filter, standard deviation $\sigma_{(star-C)}$ of the differential magnitudes of II Peg and of the check stars observed by the APT-80.

Star	HD	V mag	B−V mag	U−B mag	Time Range HJD-2400000	# Nights	# Integr.	$\sigma_{(star-C)}$ (mmag)		
v	**224085**	7.59	1.03	0.66	48948-51127	353	2913	137	105	96
ck1	223094	6.94	1.64	1.95	48948-51127	309	751	35	23	24
ck2	224895	6.82	1.21	1.16	49228-51127	302	741	35	21	23
n	223461	5.96	0.20	0.15	48843-51127	342	1097	50	33	31

Table 4. Seasonal information and photometric modulation of II Peg (see the Sect. 3 for explanation).

Time Range (HJD−2440000)	N_m	P±ΔP (days)	A (mag)	FAP (%)
2278-2336	54	6.7618± 0.0018	0.128	$2.8 \cdot 10^{-5}$
3076-3444	33	6.7372± 0.0057	0.146	0.033
4168-4271	33	6.7536± 0.1020	0.049	2.8
4483-4514	34	6.7454± 0.1620	0.063	$5.8 \cdot 10^{-3}$
4867-4937	55	6.7128± 0.0248	0.076	$1.1 \cdot 10^{-2}$
5120-5179	17	6.7209± 0.1860	0.073	19.4
5892-6098	79	6.7704± 0.0008	0.055	$1.03 \cdot 10^{-4}$
6223-6391	95	6.7536± 0.0073	0.079	$2.0 \cdot 10^{-7}$
6678-6829	62	6.7128± 0.0057	0.149	$6.22 \cdot 10^{-4}$
7441-7561	36	6.7128± 0.0133	0.140	0.57
7699-7919	54	6.7536± 0.0022	0.181	$9.0 \cdot 10^{-7}$
8095-8272	39	6.7128± 0.0012	0.054	0.24
8427-8573	36	6.6966± 0.0620	0.018	1.88
8846-9008	41	6.6886± 0.0230	0.050	2.22
9160-9359	49	6.7294± 0.0080	0.079	0.28
9541-9756	51	6.7288± 0.0056	0.095	$2.0 \cdot 10^{-5}$
9878-10089	71	6.7047± 0.0049	0.078	$1.0 \cdot 10^{-8}$
10247-10481	109	6.7065± 0.0230	0.247	$1.0 \cdot 10^{-5}$
10596-10805	112	6.7335± 0.0018	0.112	$7.1 \cdot 10^{-6}$
10996-11127	108	6.7047± 0.0005	0.135	$7.0 \cdot 10^{-7}$

$$HJD = 2442025.5 + 6.720 \times E \qquad (1)$$

where P=6.720d is the mean photometric period that was determined by minimizing the O−C residuals for the epochs of the deepest light curve minima.

4. The spot modelling technique

A map of the spot distribution on the II Peg photosphere can be derived from the analysis of the rotational modulation of the optical flux, but the solution is not unique, due to the low information content of wide-band photometry. In order to obtain a unique and stable solution, we need to assume a regularization criterion, i. e., to introduce some a priori constraints on the properties of the photospheric map. In the present approach two kinds of regularization criteria were adopted: a) the Maximum Entropy method (ME), and b) the Tikhonov criterion (T), which are described in detail by, e.g., Cameron (1992).

The star's surface is divided into elements (pixels) of $9° \times 9°$ extension. The specific intensity of the i-th pixel varies as a function of the fraction f_i of its surface covered with spots

(*spot filling factor*). More precisely, if I_u and $I_s = C_s I_u$ are the specific intensity of the unspotted photosphere of the i-th pixel, and spotted, respectively, the specific intensity of the pixel I_i will be:

$$I_i = f_i I_s + (1 - f_i)I_u \qquad (2)$$

where the brightness contrast C_s is assumed to be constant and $0 \leq f_i \leq 1$. The unspotted photospheric intensity changes over the star's surface according to the usual linear relationships for limb- and gravity-darkening (Kopal 1959).

The map of the filling factor fitting a given light curve is obtained by finding the distribution of the f_i's which gives a constrained extremum of the Maximum Entropy or of the Tikhonov functionals, respectively, subject to a χ^2 limit, set according to the accuracy of the observations. A detailed description of the adopted procedure, including a discussion of the error sources and of the accuracy, can be found in Lanza et al. (1998a).

5. Model parameters

In modelling the light curves of II Peg, it is possible to neglect completely the presence of the secondary component, because its light contribution has never been detected neither from wide-band photometry nor from spectroscopic observations. Berdyugina et al. (1998b) concluded that the secondary has an absolute magnitude $M_V \geq 8.8$, i.e., it is at least one hundred times fainter than the primary, which they classified as K2IV. In view of such an upper limit, we choose to model our system as a single star, adopting the following parameters for the K2IV component: M_V=3.8, log g=3.2, $T_{eff} = 4600$ K (Berdyugina et al. 1998b, Marino et al. 1999). A value of $i = 55°$ for the inclination of the rotation axis was assumed, i.e., intermediate between the value found by Berdyugina et al. (1998b) and the lower limit ($i \simeq 40°$) given by Vogt (1981) and Lang (1992). The star was modelled as a triaxial ellipsoid to account for centrifugal and tidal distortions and the $\nu = 0.25$ gravity-darkening coefficient was assumed (Kopal 1959, Lanza et al. 1994).

In different epochs, different values for the spot temperature were derived, ranging from T_{spot}=3300 K (Rodonò et al. 1986) to T_{spot}=3700 K (Byrne & Marang 1987). In the present analysis, we chose a fixed value of T_{spot}=3500 K, which is intermediate between the values found by the above authors and coincides with the value derived by Berdyugina et al. (1998a). By adopting the flux vs. T_{eff} calibration by Amado (1998), the adopted
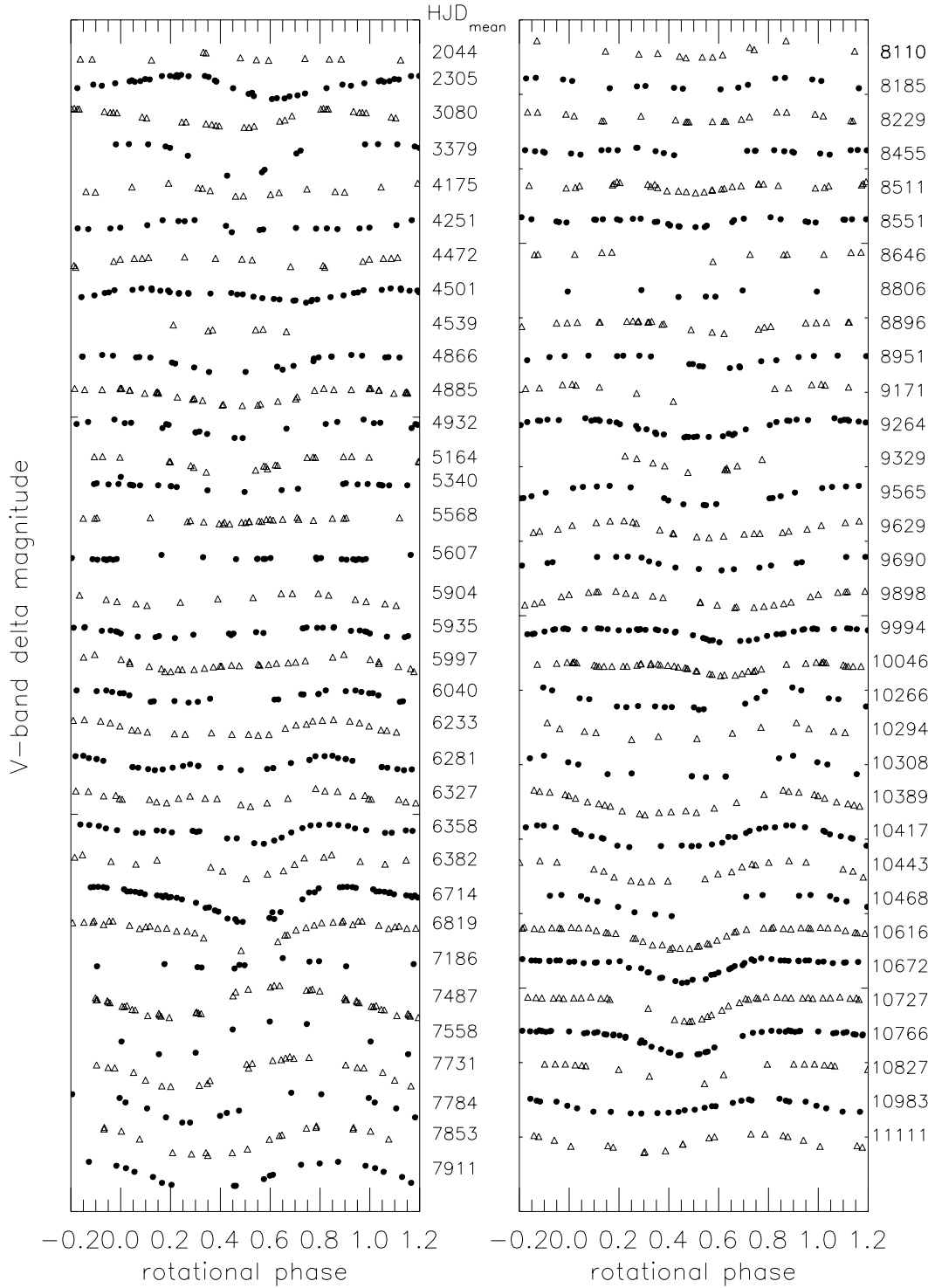
Fig. 2. The complete sequence of V-band light curves of II Peg from 1974 to 1998. Rotational phases are computed according to the ephemeris given in Eq. (1).

values for the spotted and unspotted photospheric temperatures yield to a brightness contrast $C_s = 0.973$ at $\lambda = 5500\,\text{Å}$. The limb-darkening coefficients in the V-band for the unspotted and spotted photospheres are assumed to be the same: $u_V = 0.830$ (Díaz-Cordovès et al. 1995).

The stars' unspotted magnitude $V_{un} = 7.283$ was chosen as the brightest observed over the years 1974–1998 (at HJD = 2447479.710). The complete list of stellar and model parameters is given in Table 5.
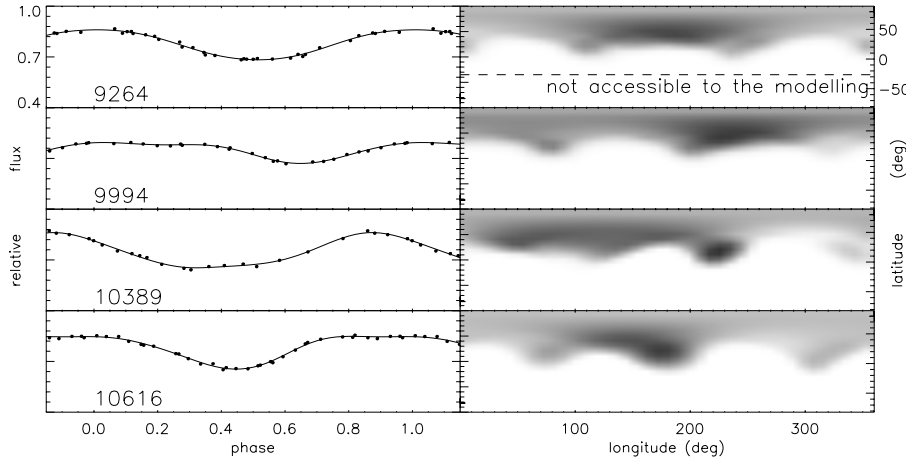
Fig. 3. Some of the V-band light curves of the analysed sequence (filled circles) fitted by the Maximum Entropy spot models (continuous lines). The HJD of the mean epoch of each light curve is indicated in the corresponding plot, respectively. The flux has been normalized to the unspotted magnitude. Phases are computed according to Eq. (1). The distributions of the spot filling factor are shown on the maps in the right hand panels. The longitude increases in the direction opposite to the stellar rotation, in such a way that the phase at which a given pixel crosses the central meridian is equal to its longitude. Spots located at latitudes below $-35°$ can not contribute to the flux, because of the star's rotation axis inclination of $55°$.
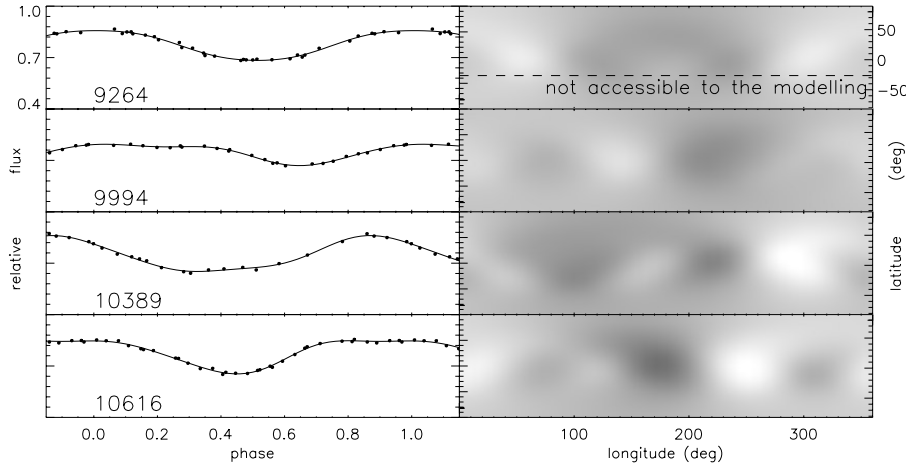
Fig. 4. The same V-band light curves presented in Fig. 3 (filled circles), fitted by the Tikhonov spot models (continuous lines). The corresponding distributions of the spot filling factor are shown on the right hand panels. The same reference frame of Fig. 3 has been adopted. The pattern in the inaccessible region is an artefact of the Tikhonov regularization that correlates the filling factors of nearby pixels.

6. Results

6.1. Photospheric maps

In Fig. 3 and Fig. 4 two illustrative examples of light curve fits are shown, together with the respective spot configurations. The Lagrangian multipliers and the χ^2 of the fits are reported in Table 6 for both the ME and T solutions, respectively. A value of the χ^2 much less than the unity simply indicates that the dispersion of the observations around the fit is significantly smaller than the assumed a priori standard deviation of 0.01 mag (see Lanza et al. 1998a for details). The derived spotted area distributions are presented as Mercator maps. On those maps the longitude increases in the direction opposite to the stellar rotation, in such a way that the phase at which a given pixel crosses the central meridian is equal to its longitude. Spots located at latitudes below $-35°$ can not contribute to the flux, because those latitudes never cross the hemisphere facing the observer and, therefore, are not accessible to the modelling.

As discussed in detail by Lanza et al. (1998a), our regularized maps should be regarded as an *intermediate step* of the analysis and used only to derive quantities which do not depend on the regularizing criterion adopted, e.g., the distributions of the spots vs. longitude, their change in time and the variations of the total spotted area.

The variations of the total spotted area vs. time appear to be very similar for both Maximum Entropy and Tikhonov solutions (see Fig. 5a). The systematic difference between the values of the area obtained with the two regularizing criteria are due to their different a priori assumptions on the properties of the spot pattern, whereas the accuracy of the *variation* of the area versus time is about 1% for both ME and T models (cf. Lanza et al. 1998a).

The Maximum Entropy modelling tends to give more compact surface inhomogeneities, minimizing the total spotted area, which ranged from 5% of the entire photosphere in 1983 up to 16% in 1998. The Tikhonov regularization tends to smooth the
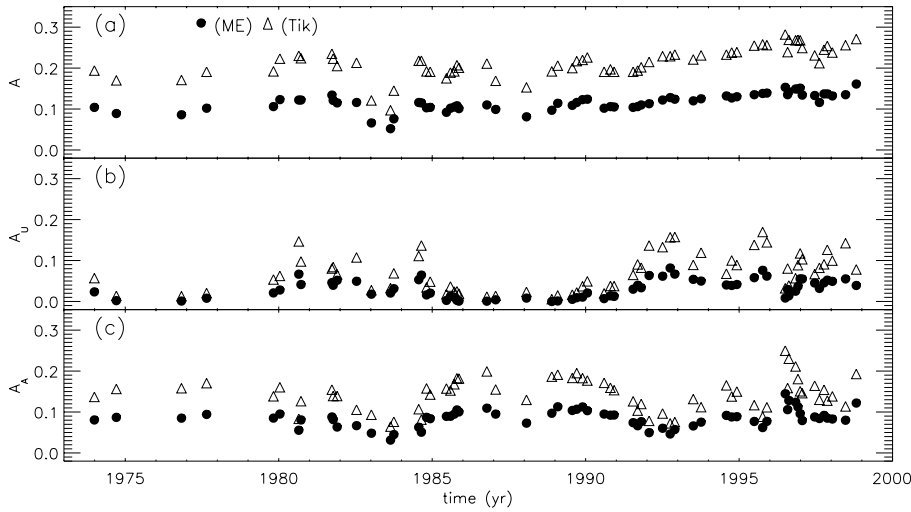
Fig. 5. a Total spotted area (in fraction of the photosphere) vs. time for the ME (filled circles) and T solutions (open triangles). **b** Area of the spot component distributed evenly in longitude vs. time for the ME and the T solutions (with the same symbols as in panel a). **c** Area of the unevenly distributed component of the spot pattern vs. time.

Table 5. Assumed stellar and model parameters to determine spot area and longitudinal distributions.

Orbital elements		
Elements		Ref.
Semi-mayor axis a_0 ($R_\odot = 1$)	6.348	1
Inclination i	$55°$	1
Eccentricity	0.0	1
Initial epoch (HJD)	2442025.5	2
Period $\langle P \rangle$ (day)	6.720	2

Stellar and Model Parameters		
Stellar Parameter	K2IV	Ref.
Ellipsois semi-axis a/a_0	0.493420	1, 3
Ellipsois semi-axis b/a_0	0.436993	1, 3
Ellipsois semi-axis c/a_0	0.411805	1, 3
Mass ($M_\odot = 1$)	0.8	1
Radius ($R_\odot = 1$)	3.4	1
Linear Limb Darkening (V band)	0.830	2
Gravity Darkening	0.25	3
Effective temperature (K)	4600	1
Starspot temperature (K)	3500	2
Unspotted V magnitude	7.283	2

1) Derived from the stellar parameters given by Berdyugina et al. (1998a, b); 2) Present study; 3) Derived according to Kopal (1959).

intensity fluctuations and gives photospheric maps almost completely covered with huge, smoothly varying spots, having a large latitudinal extension and an area ranging from 9% in 1983 to 27% of the photosphere in 1998 (see Fig. 5a).

The total spotted area (A) resulting from the modelling can be divided into two components: $A = A_U + A_A$, where A_U is the spot area uniformly distributed in longitude (Fig. 5b), and A_A the spot area unevenly distributed in longitude (Fig. 5c). The A_U component, as derived from ME maps, ranges from 0.2% at 1976.82 up to 7% at 1995.76; while it ranges from 1% to 17% at the same epochs from T maps. The A_A component, as

derived from ME maps, ranges from 3.1% at 1983.64 up to 14% at 1996.50, respectively; while it ranges from 6.4% to 25% at the same epochs from T maps.

It must be pointed out that for active stars a completely unspotted level may never become observable. Hence, the brightest observed magnitude of II Peg may differ from the true unspotted magnitude. In fact, methods based on the modelling of TiO band and OH excess give the brightest value of V_{un}=6.80 for the unspotted magnitude (Neff et al. 1995). Therefore, solutions with ME and T regularizations were also computed adopting the value of V_{un}=6.80. The behaviour of the total area A, as well as of its A_U and A_A components, appears unchanged, but the total spotted area increases by factors of 15% and 25% in the ME and T maps, respectively. The value of the A_A component remains unchanged within 1%, because the spot area unevenly distributed in longitude depends primarily on the light curve amplitude and not on the unspotted light level.

6.2. Modulation of the spot area and activity cycle

A periodogram analysis of the variations of the total spotted area A and of its two components A_U and A_A versus time was performed using the prescription by Horne & Baliunas (1986). The total area was found to vary with a periodicity of ~ 8.5 yr and FAP of 1.8%. Its two components A_U and A_A show a better defined modulation, with periods of ~ 13.6 yr and ~ 9.5 yr and FAP of 0.006% and 0.2%, respectively. After filtering the primary periodicity, secondary periodicities were detected for both components, with periods of ~ 2.8 yr and ~ 4.3 yr and FAP of 2.5% and 0.03%, respectively. The detected periodicities are quite reliable, because at least two complete activity cycles were observed, ruling out the possibility of spurious fluctuations.

Since II Peg does not show eclipses and the contribution of the secondary to the integrated light is negligible, all the modulation in the optical band can be attributed to surface inhomogeneities, such as starspots, and we may analyse the entire photometric data set to look for independent confirmation of the detected activity cycles. To this purpose, we defined three pho-

Table 6. The Lagrangian multipliers and the χ^2 of the light curve fits with ME and T regularizing criteria, respectively.

epoch	λ_{ME}	χ^2_{ME}	λ_T	χ^2_T	epoch	λ_{ME}	χ^2_{ME}	λ_T	χ^2_T
2044.08	2.0	0.0714	80.0	0.0505	8110.62	2.0	0.8038	80.0	0.7552
2305.50	2.0	0.8125	80.0	0.8201	8185.67	2.0	0.1343	80.0	0.0978
3080.49	2.0	0.2077	80.0	0.1932	8229.47	2.0	0.2534	80.0	0.1975
3379.74	2.0	0.1870	80.0	0.1504	8455.72	2.0	0.3466	80.0	0.3318
4175.30	2.0	0.1111	80.0	0.0746	8509.81	2.0	0.6356	80.0	0.6320
4251.70	2.0	1.3167	80.0	1.2841	8551.97	2.0	0.3585	80.0	0.3540
4476.76	2.0	0.2873	80.0	0.2680	8646.01	2.0	0.0425	80.0	0.0182
4502.70	2.0	0.4096	80.0	0.3923	8806.65	2.0	0.1433	80.0	0.1342
4539.57	2.0	0.1627	80.0	0.1314	8896.75	2.0	0.1208	80.0	0.1142
4870.79	2.0	0.8385	80.0	0.8051	8951.99	2.0	0.1819	80.0	0.1678
4886.16	2.0	0.8396	80.0	0.8422	9171.82	2.0	0.1790	80.0	0.1556
4933.13	2.0	1.4281	80.0	1.3869	9264.51	2.0	0.5512	80.0	0.5177
5164.12	2.0	0.6470	80.0	0.6336	9329.74	2.0	0.2305	80.0	0.1766
5340.95	2.0	0.1515	80.0	0.1052	9565.73	2.0	0.1190	80.0	0.0773
5568.37	2.0	0.5516	80.0	0.5158	9629.12	2.0	0.1274	80.0	0.1324
5607.86	2.0	0.1675	80.0	0.1548	9690.21	2.0	0.4485	80.0	0.3091
5904.29	2.0	0.1148	80.0	0.0869	9897.22	2.0	0.1097	80.0	0.1029
5935.83	2.0	0.4567	80.0	0.4525	9997.26	2.0	0.2037	80.0	0.1899
5997.05	2.0	0.5433	80.0	0.5289	10047.15	2.0	0.2110	80.0	0.1875
6040.66	2.0	1.0801	80.0	1.0632	10266.15	2.0	0.7887	80.0	0.7869
6233.84	2.0	0.4361	80.0	0.4252	10294.53	2.0	1.4103	80.0	1.5304
6281.82	2.0	0.5464	80.0	0.5681	10308.80	2.0	0.2415	80.0	0.2179
6327.17	2.0	1.5823	80.0	1.5860	10389.13	2.0	0.5221	80.0	0.5105
6358.84	2.0	0.6301	80.0	0.5707	10417.83	2.0	0.7296	80.0	0.6867
6382.18	2.0	1.3640	80.0	1.3392	10443.68	2.0	0.5143	80.0	0.4674
6714.76	2.0	1.2111	80.0	1.2190	10468.77	2.0	0.4613	80.0	0.3769
6819.87	2.0	1.5417	80.0	1.5127	10616.40	2.0	0.4450	80.0	0.4035
7186.69	2.0	0.6614	80.0	0.6173	10672.77	2.0	0.9619	80.0	0.9754
7487.76	2.0	1.1754	80.0	1.1834	10727.56	2.0	0.2515	80.0	0.2320
7558.58	2.0	0.1029	80.0	0.0716	10766.41	2.0	0.3172	80.0	0.3067
7731.83	2.0	1.4339	80.0	1.4172	10827.14	2.0	0.1365	80.0	0.0713
7784.92	2.0	0.8546	80.0	0.7875	10983.88	2.0	0.3463	80.0	0.3471
7853.54	2.0	0.6189	80.0	0.5232	11111.65	2.0	0.4029	80.0	0.3305
7911.09	2.0	0.4496	80.0	0.4179					

Table 7. Results of the periodogram analysis of the proxy indicators for the various components of the spot area (see the text for explanation). The component asymmetrically distributed in longitude is represented by ΔV_A and A_A (derived from the ME and T models, respectively); the symmetrically distributed component is represented by ΔV_U and A_U (from the ME and T models, respectively); and the total spotted area is represented by $\Delta V = \Delta V_A + \Delta V_U$ and A (from the ME and T models, respectively).

	asym. comp.		unif. comp.		total area	
	P_1 (yr)	P_2 (yr)	P_1 (yr)	P_2 (yr)	P_1 (yr)	P_2 (yr)
Photometric parameters	10.45±0.1	3.74±0.001	14.20±0.51	6.25±0.32	9.11±0.07	3.89±0.03
T Model	9.6±0.2	4.37±0.09	13.46±0.80	2.78±0.08	8.49±0.26	1.02±0.005
ME Model	9.5±0.3	4.20±0.07	13.26±1.37	2.77±0.15	8.49±0.43	1.02±0.005

tometric indexes: a) the light curve amplitude, ΔV_A, which is related to the unevenly distributed spot areas A_A; b) the difference between the magnitude at light curve maximum and the unspotted level, ΔV_U, which is correlated with spot areas evenly distributed in longitude, A_U; and c) the total brightness variation with respect to the unspotted light level, $\Delta V = \Delta V_A + \Delta V_U$, which is a measure of the total spotted area. The total brightness variation (ΔV) shows evidence for a 9.11 yr cycle period of the total spotted area changes and a secondary period of 3.89 yr, with

FAPs of 0.02% and 8%, respectively. The modulation of ΔV_A shows principal and secondary periodicities of ~ 10.5 yr and ~ 3.7 yr, respectively, close to the corresponding periodicities found for A_A, whereas ΔV_U varies with a period of ~ 6.2 yr. It is important to notice that the above defined values of the magnitude indexes are strongly affected by the variations of the maxima and minima of the light curves, whereas the area values are derived by means of spot model fits, which take into account all the information contained in the light curves. There-
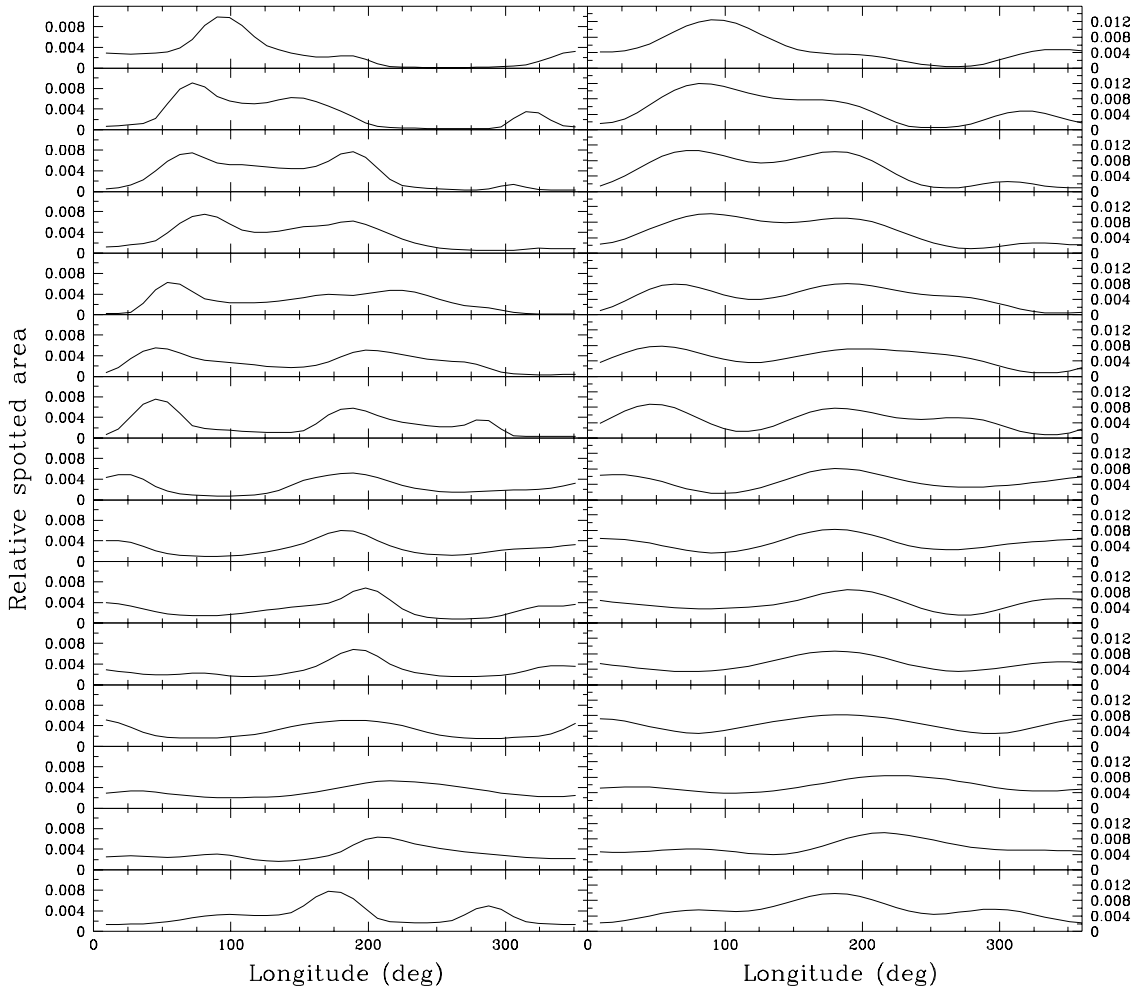
Fig. 6. The distribution of the relative spotted area vs. longitude for a sample of light curves of II Peg from 1989.56 to 1993.50 obtained from the Maximum Entropy models (left panels) and the Tikhonov models (right panels). The area unit is the photospheric area of the star.

fore, they are more reliable and less subject to possible effects of short-term fluctuations. Our results on the periodicities of the photospheric activity are summarized in Table 7.

6.3. Longitudinal distribution of the spot area

The distributions of the spotted area vs. longitude are plotted in Fig. 6 for an illustrative subset of the maps (from 1989.56 to 1993.50) obtained with the Maximum Entropy and Tikhonov criteria, respectively. The actual longitude resolution of our maps is between 50° and 70°, whereas the uncertainty in the relative spot area per longitude bin is between 10% and 40% for both regularization criteria. Such estimates were derived from the analysis of several simulated light curves, as in Lanza et al. (1998a).

In Fig. 6 we can see that the longitudes of the maxima and minima of the distributions are similar for both ME and T solutions and do not depend on the regularization adopted, because they are directly related to the minima and maxima of the corresponding light curves.

The analysis of the distribution of the spotted area vs. longitude shows that up to three well defined relative maxima are present, which can be identified with active longitudes on the photosphere of the star. The continuity of our light curve sequence allows us to identify the successive location of each longitude with little ambiguity and, therefore, to follow their time evolution.

For the sake of simplicity, since the three longitudes appear to be well separated from each other, we shall denote them as A (triangles), B and C (dots), respectively (see Fig. 7a). Spot activity is permanent in A and, from a simple inspection of the longitudinal distribution of the spotted area, it appears to vary cyclically with a period of ~ 9.5 yr. Conversely, spot activity is not continuous at the other two longitudes, B and C, but it switches from one longitude to the other with a ~ 6.8 yr cycle. The switching of activity takes about one year to be completed, during which the spot area declines steadily at the switching-off longitude and rises slowly at the switching-on longitude. As a consequence of such a gradual change, spot activity around longitudes B and C is never prominent during the switching phase. After the completion of the ~ 1.05 yr switching phase, activ-
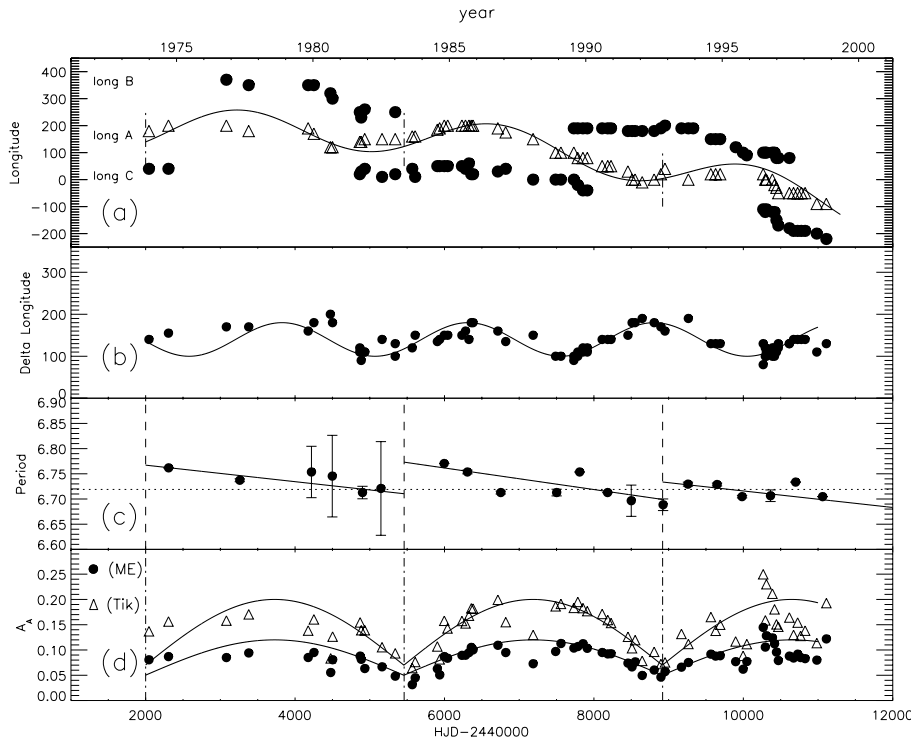
Fig. 7. a The longitudes of maximum spottedness, derived from the ME and T solutions, versus time. Longitude A is permanent, whereas B and C are alternatively active. The vertical dashes mark the beginnings of the activity cycles of longitude A. **b** The angular separation between the permanent active longitude A and the switching longitudes versus time. The continuous line is a sinusoidal fit with a period of 6.8 yr, corresponding to the period of the switching. **c** The photometric period with its uncertainty as derived by periodogram analysis (see Table 4). Continuous lines are linear best fits to the data. **d** The variation of the unevenly distributed spot area A_A versus time. The continuous lines are periodic fits with P=9.5 yr.

ity maintains at an approximately constant level for ~ 4.7 yr, which corresponds to the switching period found by Berdyugina & Tuominen (1998). Their simplified approach, based on the plot of the phases of light curve minima, was probably not capable of following the details of the switching phase, leading them to estimate a duration of only ~ 4.7 yr for the spot lifetime at each longitude.

The activity cycle in the permanently active longitude A is almost in phase with the 9.5-yr modulation of A_A, the longitude-dependent component of the spotted area (see Fig. 7d): its activity minima determine the deepest minima in the A_A modulation (i.e., at HJD $\simeq 2000, 5500$ and 9000). The B and C activity cycles are approximately in phase with the possible 4.3-yr secondary modulation of A_A. Their activity minima may determine the shallower minima in the A_A modulation (i.e., at HJD= 3600, 7300 and 10600).

The permanently active longitude A steadily migrates towards earlier rotation phases at a variable rate with a constant acceleration of $a_A = -0.56$ deg·yr^{-2}. This indicates that longitude A rotates with an average period of 6.7193 days, which is slightly shorter than the value adopted in Eq. (1) to fold the light curves, but it is equal to the rotation period found by Jetsu (1996). As shown by the continuous line, an oscillation with a period of ~ 9.5 yr is superimposed on the steady migration of longitude A. We may tentatively interpret the variation of the rate of migration as due to a change of the latitude of the spot forming region on a differentially rotating star. In the framework of such an assumption, the amplitude of the oscillation indicates a periodic migration of longitude A between latitudes with a rotation period in the range 6.7185–6.7201 days. Longitudes B and C do not show periodic changes of their migration

rate, but only some acceleration towards shorter phases during short time intervals.

The separation between longitudes B and C and longitude A is plotted in Fig. 7b and it is smaller at the switching times, varying cyclically with a period of ~ 6.8 yr, corresponding to the period of a complete switching cycle. Actually, it is the combination of the periodically changing migration rate of active longitude A and the switching of activity between longitudes B and C which appears to be responsible for the observed oscillation.

7. Discussion

The spot maps presented in the previous sections show that a large fraction of the photosphere of II Peg is spotted at any epoch. It is important to notice that the value of the total spot coverage estimated by Doppler imaging techniques always turns out of the order of 10–15% (Hatzes 1995, Berdyugina et al. 1998a, 1999). On the contrary, methods based on the modelling of TiO band and OH excess absorption give values between 35% and $\sim 50\%$ at almost the same epochs (Huenemoerder & Ramsey 1987, Neff et al. 1995, O'Neal et al. 1996, O'Neal & Neff 1997). The origin of such a discrepancy is not well understood and probably depends on the low sensitivity of the Doppler imaging techniques to the uniform spot background present on the photosphere (see Berdyugina et al. 1998a for a discussion). Our values of the spot coverage factor obtained with an unspotted magnitude of $V_{un} = 7.283$ agree fairly well with the Doppler imaging estimates, suggesting that a significant fraction of the photosphere was covered by spots even at the historical light maximum, although those spots were uniformly distributed in

longitude and did not produce any photometric modulation. Indeed, when an unspotted magnitude of $V_{un} = 6.80$ is adopted to account for such a uniform background, as suggested by Neff et al. (1995), we find coverage factors in agreement with those found by the authors who modelled molecular band features at the same epochs and also in agreement with the values found by Marino et al. (1999) by means of a newly proposed method based on contemporary multiband photometry and low resolution synthetic spectra.

The estimates of the variation of the spot area may allow us to evaluate the turbulent magnetic diffusivity η at the photosphere, in the hypothesis that the largest decrease of the total spot area is produced by a turbulent decay of the magnetic field. Adopting the approach suggested by Rodonò et al. (1995), we estimate $\eta \sim 4\pi \Delta f R^2 / \tau$, where R is the stellar radius, Δf the variation of the spot coverage factor and τ the decay time of the spot area. For II Peg we observe a decrease of the spot coverage factor, as measured by the ME models, from $\sim 14\%$ down to $\sim 5\%$ in about 1.5 yr between the end of 1982 and the beginning of 1984. Assuming a stellar radius of $R = 3.4\,R_\odot$ (Berdyugina et al. 1998b) this yields: $\eta \sim 1.5 \times 10^{11}\,\mathrm{m^2\,s^{-1}}$, which is more than one order of magnitude larger than for the Sun, but in agreement with similar estimates made for the active components of RS CVn and AR Lac (Rodonò et al. 1995, Lanza et al. 1998a). Such large values of η should be regarded as upper limits, because a smaller turbulent diffusivity may produce the same total area decay if the spot pattern consists of small solar-sized spots.

Our extended data set and detailed modelling approach allow us to address the question concerning spot activity cycles on II Peg on a firmer ground than previous studies. The present analysis shows that a modulation of the total spotted area is hardly detectable along the twenty-five years of observation, whereas the modulation of the evenly and unevenly longitude distributed spot areas are clearly detectable (cf. Fig. 5). Just the variation of these two components, occurring almost in antiphase, produces nearly flat light curves. Henry et al. (1995) found two periodicities in their spot area values with periods of $\sim 4.4 \pm 0.2$ yr and 11 ± 2 yr, respectively. Moreover, they argued that the shorter term periodicity may be related to the lifetime of each spotted area and not to the overall activity cycle. We confirm their suggestion, by noticing the similarity between such a period and the average lifetime of spots at the switching active longitudes B and C (~ 4.7 yr), which may be regarded as responsible for such a behaviour.

To summarize, we suggest that the overall spot cycle, as traced by the modulation of the A_A values, has a period of $\sim 9.5 \pm 0.3$ yr, in close agreement with the secondary periodicity of 11 ± 2 yr suggested by Henry et al. (1995). The same period characterizes the changes of the migration rate of the permanently active longitude A, and, possibly, the variation of the photometric period. In order to make this connection evident, we plotted in Fig. 7c the regression lines of the variation of the photometric period versus time during each of the three cycles covered by the available observations. Neglecting the extreme changes, probably related to the switching of activity between longitudes B and C (see below), we see that the overall
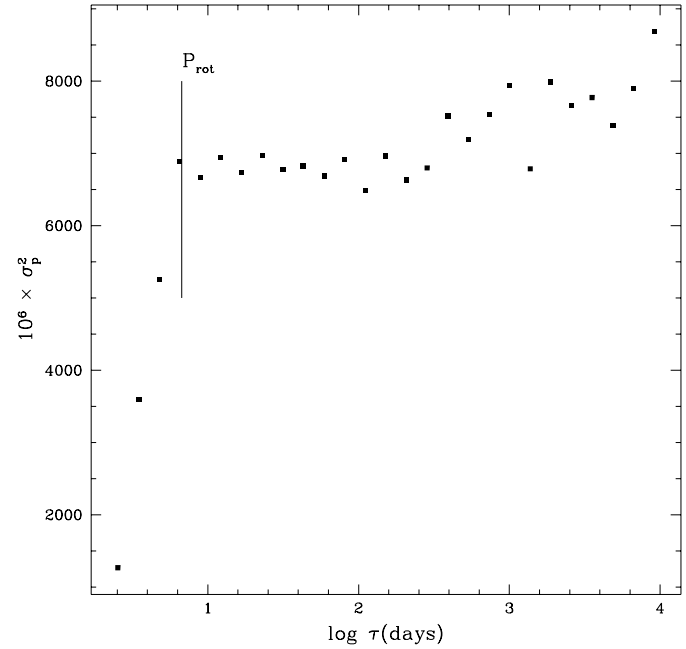
Fig. 8. The pooled variance profile of II Peg vs. the time scale τ. The time scale corresponding to the mean photometric period P_{rot} is indicated by the vertical dash.

rotation period tends to decrease steadily during the course of each cycle, jumping back at a higher value at the beginning of a new cycle. This is indeed reminiscent of the sunspot cyclic behaviour, where the latitude of spot formation moves toward the equator, i.e., toward progressively faster rotating latitudes along an activity cycle, thus producing a decrease of the photometric period (cf., e.g., Donahue 1993, Donahue & Keil 1995).

In order to clarify the connection between activity cycle and spot rotation, it is interesting to consider the possible effect of active regions' evolution on spurious variations of the photometric period. Dobson et al. (1990), Donahue & Baliunas (1992) and Donahue (1993) have proposed a method to estimate the time scale of an active region evolution, based on the analysis of the variance in photometric time series over different time scales, the so-called *pooled variance analysis*. The variance profile for the photometric data set of II Peg has been computed following the prescription of Donahue (1993) and is plotted in Fig. 8. The mean semi-amplitude of the sinusoidal fits to the observed flux modulation is $A_{ave} = 0.100$ mag. The difference between the pooled variance computed at the time scale of rotation, $\sigma^2_{rot} \simeq 7 \times 10^{-3}$ and the variance at the shortest measurable time scale $\sigma^2_{base} \simeq 1.3 \times 10^{-3}$, gives a semi-amplitude $A_p = \sqrt{\sigma^2_{rot} - \sigma^2_{base}} \simeq 0.075$, indicating that 75% of the variance observed at the rotation period is associated with the rotational modulation of the optical flux. The pooled variance levels off for timescales longer than the rotation period and begins to increase again only at $\log \tau \simeq 2.3$ ($\tau \sim 200$ days), which indicates the time scale when the evolution of the active regions begins to affect the variance of the observed flux. The value of σ^2 continues to increase up to $\sigma^2 \simeq 8.0 \times 10^{-3}$, reached at $\log \tau \simeq 3.2$ ($\tau \sim 4.7$ yr), which corresponds to the charac-

teristic lifetime of the spots at the switching active longitudes B and C. We see that these evolutionary effects do not produce a large increase of σ^2, which remains always dominated by the rotational modulation. However, the rotation periods derived by periodogram analyses may still be affected by the evolution of active regions through the shift of the phase of the light curve minima, rather than by the change of their amplitudes. Therefore, we conclude that the variations of the photometric period are a quite reliable measure of the variation of the spot rotation period, with the possible exception of those cycle phases when activity switches from one active longitude to the other. An inspection of Fig. 7 reveals, indeed, that the largest variations of the photometric period occurs with a periodicity of ~ 4.7 yr, i.e., in coincidence with the switching of activity from one longitude to the other.

Excluding the largest changes at the epochs of switching, the photometric period ranges from 6.6886 ± 0.0230 to 6.7704 ± 0.0008 days, which yields a relative differential rotation of 0.015 ± 0.0035. Henry et al. (1995) found a smaller value of 0.0045 ± 0.0004, by modelling the migration of the long lived spots in their models. An independent estimate of the differential rotation may be obtained by considering the changes of the migration rate of the active longitude A, whose rotation period is found to vary in the range from 6.7185 to 6.7201 days. In such a way we find a relative differential rotation of 0.00023, one order of magnitude smaller than the value found by Henry et al. (1995). However, such a method does not take into account the migration of the whole spot pattern, but only of the spots that form around the active longitude A.

To investigate the connection between the migration of the spots and stellar differential rotation it is of basic importance to know the latitude of the spots which contribute to most of the photometric modulation. The information is accessible to Doppler imaging, but, unfortunately, such studies are still very limited. The maps by Berdyugina et al. (1998a, 1999) do not show any significant change of the latitudes of the main spots, which were always in the range $45° - 75°$ during the 1992–1998 period. Nevertheless, during the same time interval, the photometric period varied between 6.6886 ± 0.0230 and 6.7295 ± 0.0008 days, with a relative variation of 0.0061 ± 0.0046 days. Such a value, in view of its uncertainty, is compatible with the value we find from the migration of the active longitude A and that was found by Henry et al. (1995). Differential rotation appears to be much smaller than solar, as it is typically found for RS CVn binaries (cf. Rodonò 1986, Henry et al. 1995). It is worth to note that, even without latitudinal migration of the spot pattern, small changes of the angular velocity of the spots may be observed. In particular, an increase of the rotation rate may be associated with the emergence of new spot groups, as suggested by Lanza et al. (1992) on the basis of the solar analogy.

An interesting characteristic of the activity of II Peg is the existence of long-lived active longitudes. The rotation rate of the active longitude A differs by 0.075%, on the average, from the orbital angular velocity, which implies that it takes 24.5 yr to get back to the same orbital phase during its steady migration. Therefore, its spot activity cycle of 9.5 yr does not appear to be related to the orientation of the active longitude with respect to the radius vector. The same result is found also for the switching active longitudes B and C, although Berdyugina et al. (1998a, 1999) suggested that, at each given time, the longitude closer to the line joining the centers of the two stars is more active. Such a behaviour has also been found in other RS CVn systems, as discussed by Henry et al. (1995) and Lanza & Rodonò (1999a). Specifically, there is evidence for a sector structure with three active longitudes also on the secondary component of AR Lac with the most active longitude always located close to the substellar point. The other two longitudes are less active and are located $\sim 120°$ away from the most active longitude (Lanza et al. 1998a). On HK Lac two active longitudes, separated by $\sim 110°$, have been continuously present for ~ 30 yr (Oláh et al. 1997). A different behaviour characterizes the prototype active binary RS CVn, where the active longitude, that has been observed for ~ 35 yr on the secondary component, migrates towards decreasing orbital phases with a variable rate (Rodonò et al. 1995). Recently, Berdyugina & Tuominen (1998) analysed the photometric sequences of some active stars by simply tracing the location of the light minima. They suggested that on EI Eri and II Peg (and possibly on σ Gem and HR7275) there are two active longitudes separated by $\sim 180°$, and the main activity alternately switches from one to the other with a cycle of about 10–15 yr, in a way reminiscent of the so-called flip-flop phenomenon observed on single FK Comae stars (Jetsu et al. 1993, 1994).

The complex phenomenology displayed by active longitudes in binaries and single stars can not be addressed by current mean-field dynamo models. These rely on a parameterization of small scale effects and the interaction between turbulence, rotation and magnetic fields. However, mean-field dynamo models have limited capability to explore the highly non-linear regimes that characterize very active stars. However, some illustrative models have been proposed. Moss et al. (1995) showed that in single stars non-axisymmetric magnetic fields can be excited and are stable in the non-linear regime, if the amplitude of the differential rotation is not too large ($\Delta\Omega/\Omega < 0.1$). Moss & Tuominen (1997) explored mean-field α^2 dynamo models for close binaries and found that the magnetic field is stronger preferably close to the substellar points. However, the existence of more that two active longitudes, their migration and the flip-flop switching are beyond the present modelling capability and are still waiting for a physical interpretation.

A major advance in the understanding of the dynamo action in close binaries may come from the combined study of the orbital period modulation and the spot activity, as recently pursued by, e.g., Rodonò et al. (1995), Lanza et al. (1998a), Anders et al. (1999). Following the original suggestion by Applegate (1992), Lanza et al. (1998b) and Lanza & Rodonò (1999b) proposed that the study of the orbital period modulation can provide us with information on the energy balance and the regime of the non-linear dynamo operating in close binaries. Therefore, we intend to study the orbital period changes of II Peg by means of long-term radial velocity measurements, following the method recently proposed by Frasca & Lanza (2000).

8. Conclusion

The photospheric activity of the RS CVn binary II Peg is characterized by the presence of huge spotted areas covering up to $\sim 50\%$ of the visible disk of the K2 IV star. Most of the spotted area is nearly uniformly distributed and does not produce sizeable photometric modulations or distortion of the line profiles. A periodogram analysis shows that the photometric modulation varies with a cycle of ~ 13.5 yr. The spot area unevenly distributed in longitude is mostly responsible for the photometric modulation and it is localized around three active longitudes. One of them is characterized by persistent spot activity with a cycle of ~ 9.5 yr, along which its angular velocity also varies in phase with the variation of the spot area. The other two active longitudes are not continuously active, but switches "on" and "off" with a cycle of ~ 6.8 yr. The switching is not abrupt: the dominant spot activity slowly transfers from one longitude to the other over a time interval of about one year. Therefore, the duration of the phase when only one longitude is predominantly active is on the average ~ 4.7 yr.

Differential rotation appears to be much smaller than on the Sun and its value, determined by means of periodogram analysis, turns out to be significantly higher than found from the change of the migration rate of active longitudes. Such a difference is likely to be related to the phase shift of the photometric modulation connected with the switching of activity between different longitudes.

References

Amado P.J., 1998, PhD Thesis, Armagh Observatory, Northern Ireland, UK

Anders G.J., Coates D.W., Thompson K., Innis J.L, 1999, MNRAS 310, 377

Andrews A.D., Rodonò M., Linsky J.L., et al., 1988, A&A 204, 177

Applegate J.H., 1992, ApJ 385, 621

Baliunas S.L., Boyd L.J., Genet R.M., Hall D.S., Criswell S., 1985, IAPPP Comm. 22,47

Baliunas S.L., Donahue R.A., Soon W.H., et al., 1995, ApJ 438, 269

Berdyugina S.V., Tuominen I., 1998, A&A 336, L25

Berdyugina S.V., Berdyugin A.V., Ilyin I., Tuominen I., 1998a, A&A 340, 437

Berdyugina S.V., Jankov S., Ilyin I., Tuominen I., Fekel F.C., 1998b, A&A 334, 863

Berdyugina S.V., Berdyugin A.V., Ilyin I., Tuominen I., 1999, A&A 350, 626

Bohusz E., Udalski A., 1981, AcA 31, 185

Bopp B.W., Noah P.V., 1980, PASP 92, 333

Boyd L.J., Genet R.M., Hall D.S., 1984, IAPPP Comm. 15, 20

Byrne P.B., Marang F., 1987, Ir. A. J. 18, 84

Byrne P.B., Panagi P.M., Lanzafame A.C., et al., 1995, A&A 299, 115

Cameron A.C., 1992, In: Byrne P.B., Mullan D.J. (eds.), Surface Inhomogeneities on Late-Type Stars, Springer-Verlag, Berlin, p. 33

Chugainov P.F., 1976, Iz. Kry. 57, 31

Cutispoto, G., Leto G., Pagano I., Santagati G., Ventura R., 1987, IBVS 3034

Cutispoto G., Leto G., Pagano I., 1989, IBVS 3379

Díaz-Cordovés J., Claret A., Giménez A., 1995, A&AS 110, 329

Dobson A.K., Donahue R.A., Radick R.R., Kadlec K.L., 1990. In: G. Wallerstein (ed.), The Sixth Cambridge Symposium on Cool Stars, Stellar Systems and the Sun. ASP Conf. Ser. vol. 9, p. 132

Donahue R.A., 1993, Ph.D. Thesis, New Mexico State University

Donahue R.A., Baliunas S.L., 1992, ApJ 393, L63

Donahue R.A., Keil S.L., 1995, Sol. Phys. 159, 53

Doyle J.G., Kellett B.J., Butler C.J., et al., 1992, A&AS 96, 351

Doyle J.G., Mathioudakis M., Murphy H.M., et al., 1993, A&A 278, 499

Evren S., 1988, Ap&SS 143, 123

Frasca A., Lanza A.F., 2000, A&A 356, 267

Hall D.S., Henry G.W., 1983, IBVS 2307

Hartmann L., Londoño C., Phyllips M.J., 1979, ApJ 229, 183

Hatzes A., 1995, in: K.G. Strassmeier (ed.) Poster Proceeding: Stellar Surface Structures, IAU Symp. 176, Univ. of Vienna, p. 87

Henry G.W., 1983, IBVS 2309

Henry G.W., Eaton J.A., Hamer J., Hall D.S., 1995 ApJSS 97, 513

Horne J.H., Baliunas S.L., 1986, ApJ 302, 757

Huenemoerder D.P., Ramsey L.W., 1987, ApJ 319, 392

Jetsu L., 1996 A&A 314, 153

Jetsu L., Pelt J., Tuominen I., 1993, A&A 278, 449

Jetsu L., Tuominen I., Grankin K.N., Mel'Nikov S.Yu., Schevchenko V.S., 1994, A&A 282, L9

Kaluzny J., 1984, IBVS 2627

Kopal Z., 1959, Close Binary Systems, Chapman & Hall, London

Lang K.R., 1992, Astrophysical Data, Springer-Verlag

Lanza A.F., Rodonò M., Zappalà R.A., 1992, in P.B. Byrne and D.J. Mullan (Eds.), Surface Inhomogeneities on Late-type Stars, LNP 397, Springer-Verlag, Berlin, p. 298

Lanza A.F., Rodonò M., Zappalà R.A., 1994, A&A 290, 861

Lanza A.F., Catalano S., Cutispoto G., Pagano I., Rodonò M., 1998a, A&A 332, 541

Lanza A.F., Rodonò M., Rosner R., 1998b, MNRAS 296, 803

Lanza A.F., Rodonò M., 1999a, in: C.J. Butler, G.J. Doyle, Solar and Stellar Activity: Similarities and Differences, ASP Conf. Ser. vol. 158, p. 121

Lanza A.F., Rodonò M., 1999b, A&A 349, 887

Lines R.D., Louth H., Stelzel H.J., Hall D.S., 1983, IBVS 2308

Marino G., Rodonò M., Leto G., Cutispoto G., 1999, A&A 352, 189

Messina S., 1998, PhD Thesis, Univ. of Catania, Italy

Mohin S., Raveendran A.V., 1993, A&A 277, 155

Moss D., Barker D.M., Brandenburg A., Tuominen I., 1995, A&A 294, 155

Moss D., Tuominen I., 1997, A&A 321, 151

Nations H.L., Ramsey L.W., 1981, AJ 86, 433

Neff J.E., O'Neal D., Saar S.H., 1995, ApJ 452, 879

Oláh K., Kővári Zs., Bartus J., et al., 1997, A&A 321, 811

O'Neal D., Saar, S.H., Neff J.E., 1996, ApJ 463, 766
O'Neal D., Neff J.E., 1997, AJ 113, 1129
Poe C.H., Eaton J.A., 1985, ApJ 289, 644
Raveendran A.V., Mohin S., Mekkaden M.V., 1981, MNRAS 196, 289
Rodonò M., 1986, in J.-P. Swings (ed.), Highlights of Astronomy, Reidel Publ. Co., Dordrecht, p.429
Rodonò M., Cutispoto G., Pazzani V., et al., 1986, A&A 165, 135
Rodonò M., Cutispoto G., 1992, A&AS 95, 55
Rodonò M., Lanza A.F., Catalano S., 1995, A&A 301, 75

Rucinski S.M., 1977, PASP 89, 280
Scargle J.D., 1982, ApJ 263, 835
Strassmeier K.G., Hall D.S., Boyd L.J., Genet R.M., 1989, ApJS 69, 141
Strassmeier K.G., Bartus J., Cutispoto G., Rodonò M., 1997, A&A 125, 11
van den Oord G.H.J., de Bruyn A.G., 1994, A&A 286, 181
Vogt S.S., 1981, ApJ 247, 975